COVER LETTER FOR SUBMISSION OF MANUSCRIPT

Journal of Inorganic and Organometallic Polymers and Materials

Dear Editor-In-Chief,

SUBMISSION OF A MANUSCRIPT FOR EVALUATION

This is to submit a full manuscript titled "**Hydrophilic Quaternary Trimethyl Chitosan Stabilized Silver Nanoparticles: Synthesis, Characterization and Antimicrobial Activity**" for publication in Journal of Inorganic and Organometallic Polymers and Materials.

With the submission of this manuscript, I would like to undertake that the aforementioned manuscript has not been published elsewhere, accepted for publication elsewhere or under editorial review for publication elsewhere.

The authors declare no conflict of competing/financial interest

Thank you.

Prof. Sheriff Adewuyi,

(Corresponding Author)

Hydrophilic Quaternary Trimethyl Chitosan Stabilized Silver Nanoparticles: Synthesis, Characterization and Antimicrobial Activity.

Yakubu Adekunle Alli[a,b], Sheriff Adewuyi[a*], Saliu Alao Amolegbe[a], Sabu Thomas[b]

[a]Department of Chemistry, Federal University of Agriculture Abeokuta, Ogun State Abeokuta, 2240, Nigeria.

[b]School of Energy Materials and International and Inter University Centre for Nanoscience and Nanotechnology (IIUCNN), Kottayam, Kerala, 686560, India.

*Corresponding author: adewuyis@funaab.edu.ng (Sheriff Adewuyi)

Abstract

Antimicrobial resistance (AMR) endangers the effective management of an increasing range of bacterial and fungal infections, alternative antimicrobial drugs are thus, expedient. In this study, Quaternary Trimethyl Chitosan (QTMC) was prepared by improved two step reductive methylation of Chitosan (CTS) employed as a capping agent for the synthesis of silver nanoparticles (QTMC-AgNPs). The hydrophilic QTMC and QTMC-AgNPs were characterized using various analytical and spectroscopic techniques. The Proton Nuclear Magnetic Resonance (^{1}HNMR) was used to determine the degree of quaternization (DQ) and degree of dimethylation (DT) of QTMC as 63.33 and 11.75 % respectively. The Ultraviolet-Visible (Uv-Vis), Attenuated Total Reflection Fourier Transform Infrared (ATR-FTIR), X-ray Diffraction (XRD), Energy Dispersive X-ray (EDS) and X-ray Photoelectron (XPS) Spectroscopic results evidently indicated high degree of quaternization of CTS and configured QTMC-AgNPs. Thermogravimetric Analysis/Derivative Thermogravimetry (TGA/DTG) were used to study the decomposition process of QTMC and QTMC-AgNPs. The surface morphological difference of QTMC and QTMC-AgNPs was explored via Scanning Electron and High-Resolution Transmission Electron Microscopies (SEM and HR-TEM) whereas particle size distribution was analyzed using Dynamic Light Scattering. Furthermore, HR-TEM indicated QTMC stabilized AgNPs with average nanoparticulate size of 10 nm while DLS revealed 12.5 nm. This well-tailored QTMC-AgNPs exhibited strong antibacterial and antifungal activities against the tested bacteria and fungi infections.

Keywords Quaternary trimethyl chitosan. Chitosan. Silver nanoparticles. Antibacterial. Antifungal.

1 Introduction

Adaptation of microorganisms, especially bacteria and fungi to existing antimicrobial drugs, usually results into drug inefficiency and persistent infections, with a subsequent increase in the risks of severe disease and mode of transmission [1]. In recent time, AMR has become major global challenge to the health sector, endangering the ability to prevent and cure a wide range of infectious diseases [1 - 3]. It has been projected that up to ten million deaths will be recorded per year due to AMR starting from 2050 with total global cost of up to $USD 100.2 trillion [2, 4]. This implies that the AMR may pose severe global threat in future more than the current severe acute respiratory syndrome coronavirus 2 (SARS-COV-2) if the entire world fails to expedite action. According to World Health Organization's (WHO) report, among the bacteria with alarming resistance levels are E. *coli,* S. *aureus* and K. *pneumonia* [2, 4]. Also, among the fungal diseases, dry root rot of consumable vegetable such as tomatoes, peppers, caused by *S. rolfsii* and *F. oxysporum* is of major concern occasioning high economic losses in vegetable [5]. The development of active nanofungicides to control this soil borne pathogens is highly crucial.

In the quest for alternative strong antimicrobial agents, metallic nanoparticles, especially, silver nanoparticles (AgNPs) have gained attention momentously, due to its uncommon physical, optical, mechanical, magnetic, biological and chemical properties. AgNPs are well-known to exhibit a strong antimicrobial activity against various microorganisms such as bacteria, viruses, and fungi due to their smaller size and large surface area [6]. However, the role of a stabilizing agent is highly essential to prevent agglomeration [7]. In this regard, the role of chitosan (CTS), which is a cationic amino polysaccharide copolymer of glucosamine and N-acetyl glucosamine [8, 9], as a strong stabilizing agent of metal nanoparticles has already been established [10]. Also, the non-toxicity, biodegradability, film forming ability of chitosan and the ease with which it can be functionalized with other materials coupled with its inherent and fascinating antimicrobial properties further makes it an excellent candidate [10 - 12]. The obvious presence of free amine and hydroxyl groups in chitosan is responsible for the greater reactivity and stability when compared with cellulose [13]. The insertion of functional groups into the chitosan polymer matrix may improve its capacity of interaction with metallic ion by complexation [14]. The free amino group available in the chitosan structure enables a variety of chemical modifications and substitution processes like carboxylation, acylation, sulphation, Schiff's base formation, enzymatic substitution, metal chelation, cyanoethylation, nitration, phosphorylation, e. t. c. [15]. However, a major drawback is its underutilization owing to low solubility in neutral and alkaline solutions [16, 17].

In order to overcome the limitation, QTMC which is a water-soluble CTS derivative has been focused. A major advantage of QTMC is that it retains the original key features of CTS with improved hydrophilicity [9,18]. What is more, its biocompatibility, biodegradability, antibacterial activity, catalytic activity and

mucoadhesivity are greatly enhanced [9, 16], owing to increased positive charges on the polysaccharide chain length. Functional preparatory technique has been established for the preparation of QTMC, which mainly involved the reaction of CTS with excess iodomethane in the presence of N-methyl-2-pyrrolidone, sodium iodide under strongly basic conditions at 60 ℃ [16, 17, 19]. Chang and co-workers [17] however, further extended the reaction step by replacing the chloride counter ions of TMC with nitrate to form quaternary trimethyl chitosan nitrate (TMCN). The group adopted this step, in order to avoid AgCl precipitation before AgNPs formation in the Ag^+ reduction reaction intending high yield of the AgNPs.

Although silver nitrate is more soluble in water, however, the extra step addition in the preparation of QTMC will obviously reduce its yield. In order to attain lofty preparation of QTMC and improved nanocomposite formation with AgNPs, QTMC-AgNPs can be further made in an environmentally friendly manner by the chemical reduction of silver ions in an agitated aqueous medium below room temperature without heating or photo-radiation. Hitherto, this study therefore, aims to explore the effect of improved water soluble QTMC and QTMC-AgNPs, with positively charged surfaces on both AMR gram-positive and gram-negative bacteria and two plant fungi. QTMC-AgNPs were synthesized via chemical reduction approach and the nanocomposite formation conditions based on the concentrations of the stabilizer (QTMC) were investigated. The physical and chemical properties were characterized by UV-visible spectroscopy, ATR-FTIR spectroscopy, ^{1}HNMR, SEM-EDS spectroscopy, dynamic light scattering, TGA/DTG analysis, HR-TEM, XPS and X-ray diffraction. Antibacterial activities of QTMC-AgNPs nanocomposites against gram-negative (*Escherichia coli*) and gram-positive (*Staphylococcus aureus*) bacteria were measured using both disc diffusion method and broth microdilution method to determine the minimum inhibitory concentrations (MICs). In turn, antifungal properties of these nanocomposites were tested against *S. rolfsii* and *F. oxysporum* and the results obtained are herein reported.

2 Materials and Methods

2.1 Materials

Chitosan (degree of deacetylation (DD): 75%), Sodium Iodide (Molecular Weight: 149.89, Assay: 99.00 – 100.50%), sodium borohydride (Molecular Weight: 149.89, Assay: 98.00 – 102.50%) were purchased from HiMedia Laboratories Pvt., Ltd. (Mumbai-400086, India). Silver nitrate (Assay: 99.00%) was procured from Merck Life Science Private Limited, India. Sodium iodide, Sodium hydroxide, Sodium chloride and N-methyl-2-pyrrolidone were procured from Sigma-Aldrich (St. Louis, MO, USA). Resazurin dye was a gift from School of Biological Science, Mahatma Gandhi University, Kerala, India.

2.2 Synthesis of QTMC-AgNPs

A single step reaction method was adopted for the preparation of QTMC-AgNPs using modified a previously reported procedure (Scheme 1). In a typical reaction, an aqueous solution of silver nitrate (20 mL, 60 mM) was added to a dilute solution of QTMC (40 mL, concentration varied from 4.96 to 6.2 mM, $AgNO_3$: saccharide unit ratios were 1:12, 1:14, 1:16) with vigorous stirring on an ice-water bath for 30 min. Thereafter, a freshly prepared and cooled $NaBH_4$ aqueous solution (1.2 mL, 0.1 M) was added into the reaction mixture [20, 21]. The resultant solution immediately turned from almost colorless solution to dark color. The solution was subjected to constant stirring for the duration of $1\frac{1}{2}$ hours and a dark color observed. After the synthesis, the resultant product was carefully centrifuged and decanted under controlled conditions. Thereafter, the solid sample was rinsed with acetone and double distilled water and dried under in a vacuum pump at 40 ℃ overnight.

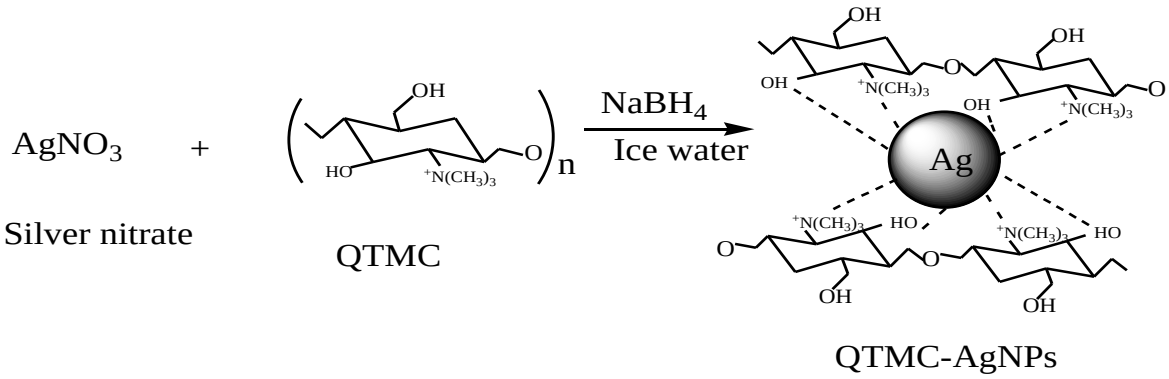

Scheme 1 Synthetic pathway of QTMC-AgNPs

2.3 Instrumental measurements

^{1}H NMR spectrum of QTMC was determined on Bruker Advance III 400 MHz by measuring approximately 10 mg of QTMC in a clean NMR tube and dissolved in ~0.5 mL of deuterated water (D_2O). The UV-Visible spectra of CTS, QTMC, QTMC-AgNPs were all recorded on UV-Visible Spectrometer (Thermo Scientific Evolution 201 and Shimadzu UV-2600). The UV-Vis spectra were measured within the range of 200 to 800 nm. Samples were run in a glass cuvette and Milli-Q water was used in a reference cell. All the concentrated samples were diluted 50 folds in Milli-Q water before characterization. FTIR spectra of CTS, QTMC, QTMC-AgNPs were all recorded on a single reflection Attenuated Reflection- Fourier Transform Infrared (ATR-FTIR) spectrometer (PerkinElmer Spectrum Two) in a scan range of 4000–400 cm^{-1}, and resolution of 4 cm^{-1}. The thermogravimetric (TGA/DTG) analysis of CTS, QTMC, QTMC-AgNPs were performed on a Thermogravimetric Analyzer (SDT Q600 V20.9 Build 20, Universal V4.5A TA Instrument, IUIC, Mahatma Gandhi University,

India) at a heating rate of 10 ℃ min^{-1} from 40 to 700 ℃ under nitrogen purge of 50 mL min^{-1}. The X-ray diffractograms of QTMC-AgNPs, was recorded on an X-ray diffractometer (Brucker AXS D8 advance®, Karlsruhe, Germany). Diffractograms were scanned in a scattering range from 20 to 80° (2) with resolution of 0.02° and scanning speed of 2.0° min^{-1}, applying an accelerating voltage of 40 kV, and a current intensity of 35 mA. Dispersions of QTMC-AgNPs, was visualized by High-Resolution Transmission Electron Microscope (HR-TEM, JEOL, JEM-2100, MA, Japan). Samples were carbon-coated on copper grids and stained with phosphor tungstic acid (2%, w/v), air-dried and viewed under HR-TEM. Photomicrographs were captured at 200 kV at different magnifications. Scanning electron microscopy (SEM, JSM-6390®, Jeol DATUM Ltd., Tokyo, Japan) was employed to examine the morphology of CTS, QTMC and QTMC-AgNPs. Samples were sputter-coated with a thin layer $(400A)^0$ of gold. Photomicrographs were captured at 10 kV with a magnification of 500 and above. The particle size distribution of QTMC-AgNPs was performed on Dynamic Light Scattering (Mark-Houwink-Sakurada parameters, India). The quantitative and chemical state of QTMC-AgNPs information was examined on X-ray Photoelectron Spectroscopy (XPS, PHI 5000 VersaProbe III, physical electronics) located at Institute Instrumentation Centre, Indian Institute of Technology Roorkee.

2.4 In Vitro Susceptibility Test (Disk Diffusion Method)

The antibacterial activity of QTMC-AgNPs was tested against gram positive, *S. aureus* and gram negative, *E. coli* bacteria pathogens by standard well diffusion in Muller Hinton Agar (MHA) plates. Pure cultures of bacterial pathogens were grown in trypticase soy broth (TSB) (Himedia) at 37 ℃ for 18-24 hours. The turbidity of bacterial cultures was adjusted to 0.5 McFarlands standard. The MHA plates were inoculated by swabbing the bacterial pathogens to create a confluent lawn of bacterial growth. Wells were made on the Muller- Hinton agar plates using a gel puncture and 50 µL of QTMC-AgNPs was added to separate wells. After incubation for 24 hours, the diameter of zone of inhibition was measured [**22** - **26**].

2.5 Preparation of Resazurin Based Microtiter Assay for MIC and MBC Test

The MIC test was performed in 96-well round bottom microtiter plate using standard broth micro dilution methods. *E. coli* and *S. aureus* were cultured in muller Hinton broth overnight and a final turbidity was adjusted to 0.5 McFarland Standard. For the MIC test, the synthesized QTMC-AgNPs was added into Mueller Hinton broth by serial two-fold dilutions from a concentration of 500 to 0.49 µg/mL. Growth and sterility control wells were maintained in each microtitre plate and the plates were incubated for 24 hrs at 37 ℃ in a bacteriological incubator. Column 1 of the microtiter plate contained the highest concentration of QTMC-AgNPs. Column 12 served as positive control (medium and bacterial inoculums) while row one

and two served as negative control for *E. coli* and *S. aureus* respectively. Each well of the microtiter plate was added with 30 µL (0.015 %) of the resazurin solution and incubated at 37 °C for 2-4 hrs for the observation of color change. Blue/purple color indicated no bacterial growth while pink/colorless indicated bacterial growth (Fig. 6). The MIC value was taken at the lowest concentration of antibacterial agents that inhibits the growth of bacteria (color remained in blue /purple) [27, 28]. Also, minimum bactericidal concentration (MBC) was determined by directly taking the content of wells with concentration higher than the MIC value in three plates. The MBC value was carefully examined when there was no growth of colony from the directly plated wells. In addition, the contents of the wells showing indication of growth inhibition were serially diluted to quantify an end-point killing of the bacteria.

2.6 Antifungal assay

The antifungal activity of QTMC-AgNPs against *F. oxysporum* and *S. rolfsii* using poison food technique in vitro adopting the medium of potato dextrose agar (PDA) [5, 29, 30].

Typically, graded concentration (50 µg/mL) of QTMC-AgNPs was incorporated into potato dextrose agar (PDA) plates. Thereafter, a nine millimeter disc of the actively growing pathogen of *F. oxysporum* and *S. rolfsii* from a 7 days old culture were placed at the center of each PDA plate containing the QTMC-AgNPs. The PDA plates inoculated with each fungal agar without QTMC-AgNPs served as a control. The diameters (D) of the fungal growth were measured in millimeters after ten days of inoculation by incubating the petri plates at 28 ℃ and the percentage of growth inhibition was determined using the following equation (Eq. 1) [30].

$$\text{Growth inhibition (\%)} = \left[\frac{\text{G-control - G-test}}{\text{G-control}} \right] \text{X } 100 \quad \text{.....1}$$

where, G-control is the radial growth of fungal mycelia on the control plate and G-test is the radial growth of fungal mycelia on the plate treated with silver nanoparticle.

3 Results and discussion

3.1 Characterization

The ^{1}H NMR spectrum of QTMC obtained after two step methylation of CTS is presented in Fig. 1. The spectrum clearly showed peaks at 3.03 and 2.82 ppm assigned to H of N-trimethyl group $^{+}N(CH_3)_3$ and H of N-dimethyl group $N(CH_3)_2$, respectively. The characteristics peaks observed between 4.6 to 5.4 ppm can be assigned to H proton at C1 the peak at 2.02 ppm assigned to H of N-acetyl group [$NCOCH_3$]. These assignments are in good agreement with that reported literature by previous studies [16, 17, 19, 20]. The

degree of quaternization and degree of dimethylation were evaluated according to our previously reported procedure [21]. The DQ% and DT% of QTMC as calculated from proton NMR spectra were 63.33 and 11.75% respectively. These results further confirmed that the main product is the quaternary derivatives [16, 17, 19, 20].

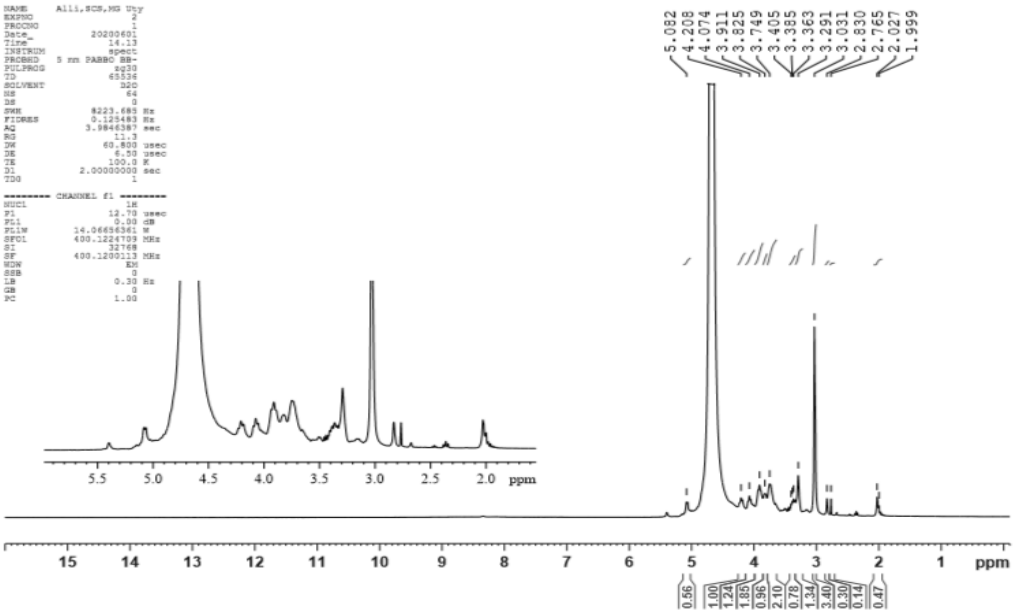

Fig. 1 ^{1}H NMR spectrum of QTMC

The solubility test of CTS and QTMC (Fig. 2) were repeatedly carried out according to previously reported procedures [8, 16]. The test revealed that CTS, initially tested, is insoluble in water and at neutral pH whereas it ionized at acidic pH and becomes soluble. The formation of quaternary salt and introduction of hydrophilic groups on the CTS backbone significantly enhanced aqueous solubility of QTMC (96.63%) which was approximately 25-folds greater than CTS (4%). The relative solubility of CTS notably decreased (97 at pH 2; 88 at pH 6) to almost insoluble levels at pH values higher than 6 (7.32 at pH 7; 3.5 at pH 12). In contrast, QTMC exhibited a higher relative solubility over the entire pH range (100 % at pH 2 to 91.4 at pH 12). Thus, the controlled introduction of functional hydrophilic groups with positive charges by two step trimethylation of CTS drastically enhanced the solubility over the entire pH range, especially in neutral and basic pH range (7–12) compared to ordinary CTS [8, 16].

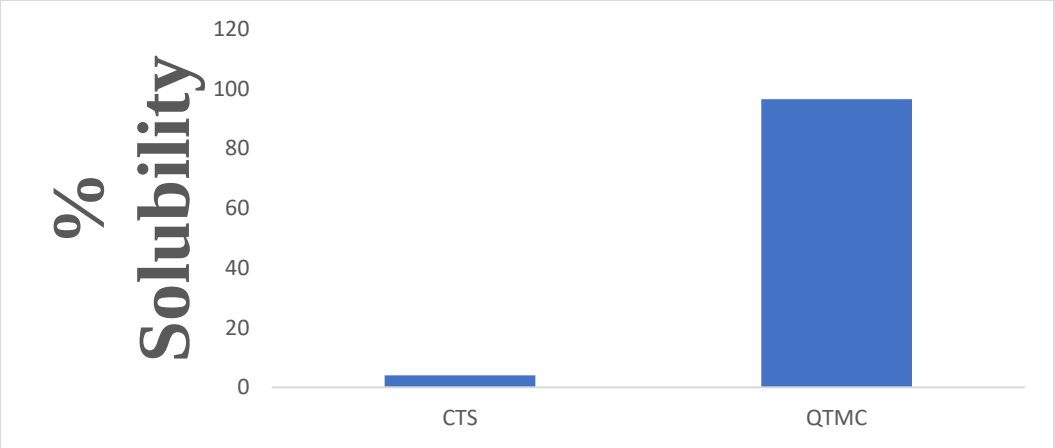

Fig. 2 Percentage saturation of solubility of CTS and QTMC

The UV-Vis spectrum of CTS shows a prominent absorption peak at 220 nm (Fig. 3a). Expectedly, no absorption peaks at the range of 300 – 800 nm. This observation is in accordance with previous studies often used for chitosan identification [12]. In contrast, the UV-Visible spectrum of QTMC (Fig. 3b) displayed characteristic bands at 218, 290 and 360 nm which is completely different from the absorption spectrum of native CTS. The formation of colloidal suspensions of QTMC-AgNPs was first evident from visual inspection of the reagent mixtures under magnetic stirring (the colour changed from colourless to dark solution). QTMC-AgNPs showed a very sharp characteristic absorption peak at 401 nm (Fig. 3c) similar to previous reported studies that adopted different routes for the preparation of the nanocomposite [6, 17, 20].

Furthermore, the effect of initial concentration of QTMC on the formation of QTMC-AgNPs was evaluated and the absorbance increased as the concentration of QTMC saccharide unit increases with slight blue shift (Fig. 3d). This is attributed to an increase in the number of the capped silver nanoparticles. This implies that the concentration of QTMC played a significant role in the optical property of the synthesized QTMC-AgNPs nanocomposites [6, 20, 31].

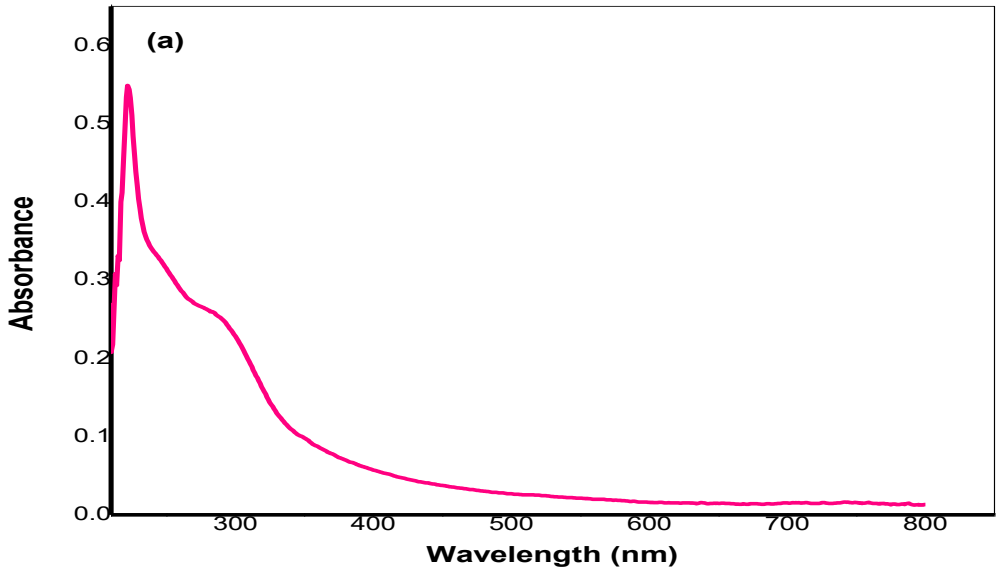
(a)
Absorbance
0.0
0.1
0.2
0.3
0.4
0.5
0.6
300
400
500
600
700
800
Wavelength (nm)

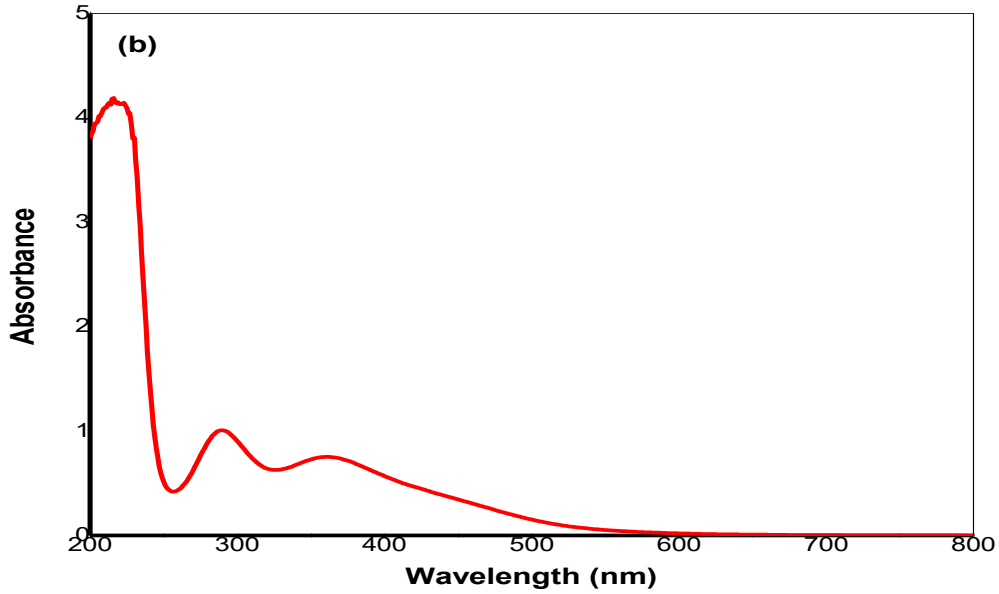
(b)
Absorbance
0
1
2
3
4
5
200
300
400
500
600
700
800
Wavelength (nm)

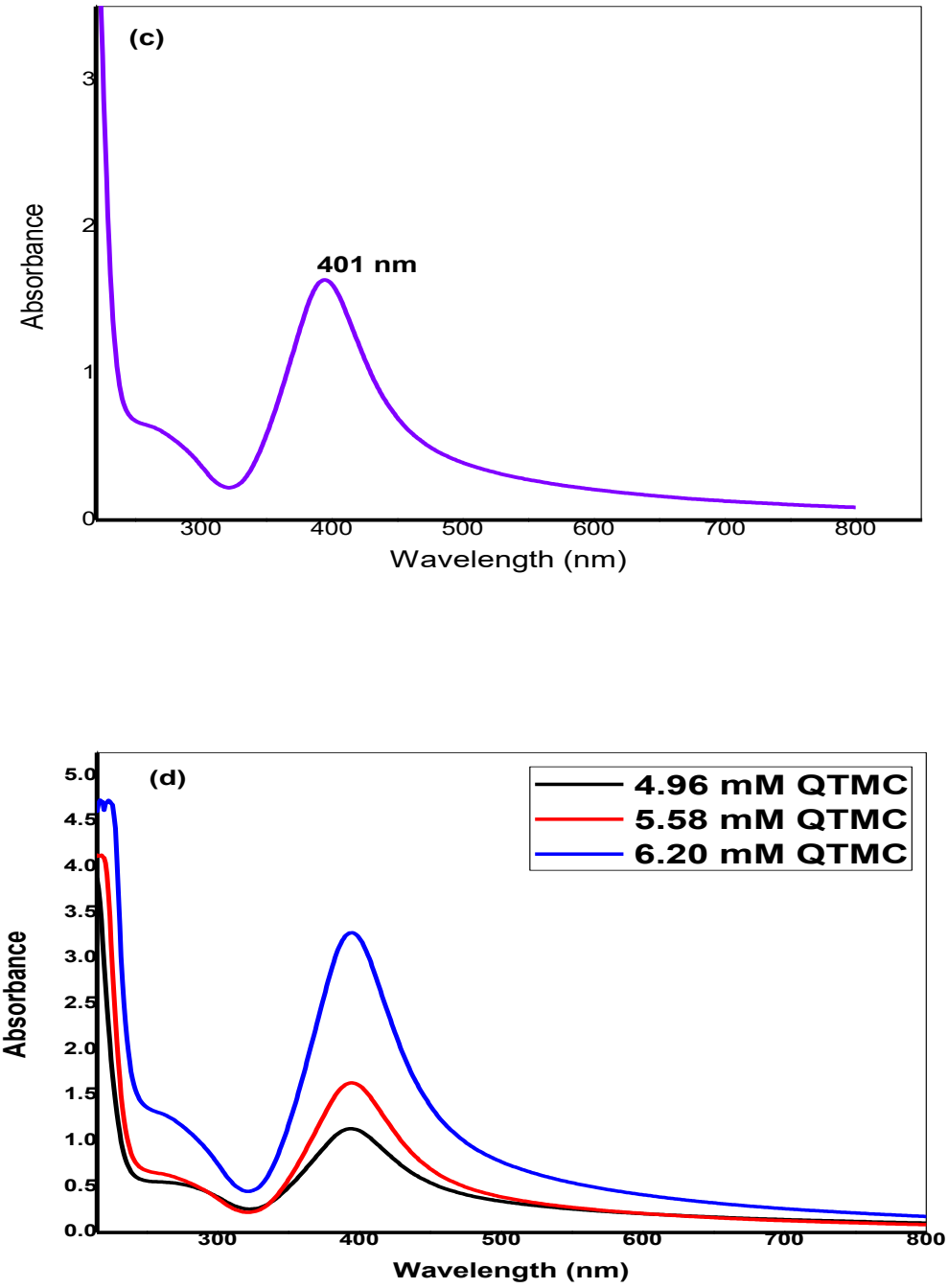

Fig. 3 UV-Visible spectral of (a) CTS (b) QTMC (c) QTMC-AgNPs (d) QTMC-AgNPs at different concentration of QTMC

The ATR-FTIR spectra of CTS, QTMC and QTMC-AgNPs are presented in Fig. 4. The evidence of quaternization of CTS is suggested by a characteristic band at 1473 cm^{-1}which is present on the spectrum

of QTMC. This can be assigned to the angular deformation (asymmetric stretching) of C-H bonds of methyl groups (CH_3 antisym deformation), which is completely absent on the spectrum of CTS. Also suggesting CTS modification (QTMC formation) is the absence of the characteristic band centered at 1577 cm^{-1} in the spectrum of QTMC, which was assigned to the angular deformation of N-H bonds of the amino groups on CTS [16, 20, 32]. In addition, the repositioning of the band at 2876 cm^{-1} on the CTS spectrum to the 2935 cm^{-1} on the QTMC spectrum is assigned to the axial deformation (symmetric and asymmetric) of C-H bonds, due to the presence of methyl carbons on the QTMC structure. This observed bands shift to higher wavenumber on the QTMC spectrum, compared to that of CTS can be ascribed to the presence of a high number of C-H bonds on QTMC backbone [16, 20, 32]. A small and broad band appeared at 2108 cm^{-1} on the QTMC spectrum is attributed to the presence of ammonium ion. The intensity of band centered at 1647 cm^{-1} on CTS spectrum is reduced to 1641 cm^{-1} on the QTMC spectrum (assigned to the axial stretching of C-O bonds of the acetamide groups, referred to as amide I band) and this may be due to intermolecular hydrogen bonding. The characteristic bands of primary and secondary alcohols at 1151 and 1027 cm^{-1} on CTS spectrum are retained at 1151 and 1032 cm^{-1} on spectrum of QTMC, which signifies that the substitution took place only at amino groups and not at C-3 or C-6 on the CTS [16, 17, 20].

In comparison with the spectrum of QTMC, the disappearance of $–CH_2$ and - CH_3 vibrations at 2935 cm^{-1}, 2888 cm^{-1} and 1473 cm^{-1} in the spectrum of the QTMC-AgNPs, shows the partial loss of the C–H vibrations assigned to the methyl groups modified on the C2–NH_2 of native CTS. This observation is in line with the previously reported literatures [16, 20, 32].

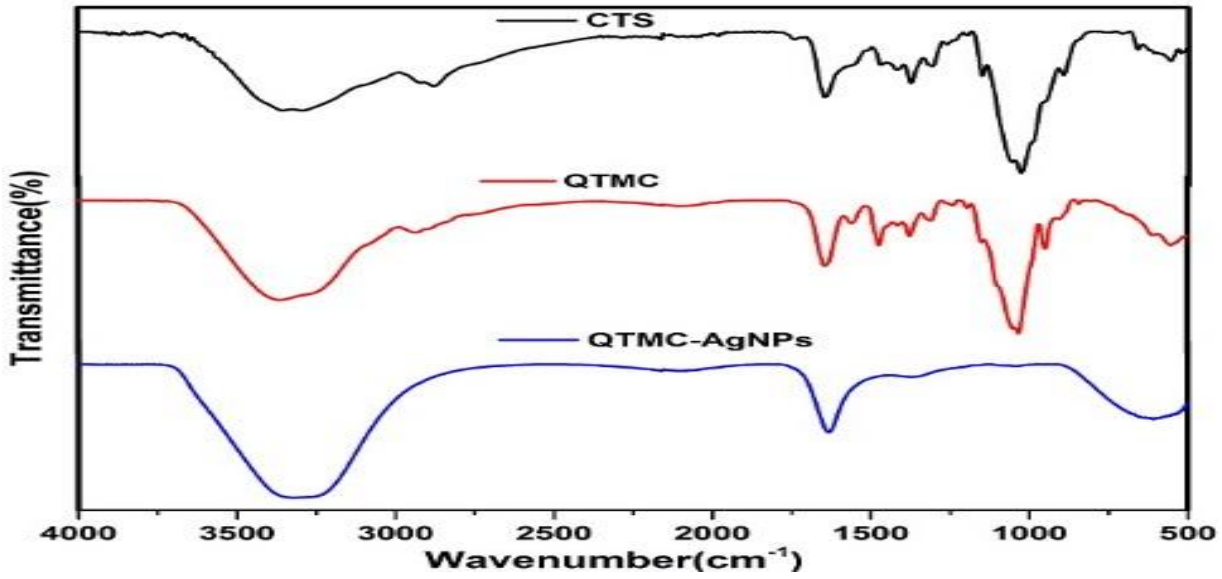

Fig. 4 ATR-FTIR spectra of CTS, QTMC and QTMC-AgNPs

The phase and crystallinity of the sample was investigated by X-ray diffraction. The XRD patterns for synthesized QTMC-AgNPs showed that four main characteristic diffraction peaks for Ag were observed at 2θ = 38.021, 44.5, 64.3 and 77.7º which correspond to the (111), (200), (220) and (311) crystallographic planes of face centered cubic (fcc) Ag crystals, respectively (Fig. 5). The most intense peak at 2θ = 38.021 is obtained along (111) reflection plane and it is very close to the position of the strongest line (2θ=38.11) of the reference Ag (File No: 04-0783) [33 - 35]. The XRD patterns thus clearly illustrated that the QTMC-AgNPs formed in this study were crystalline in nature. The main crystalline phase was silver, and the XRD profile also exhibited the presence of an additional peak, appearing at 2θ value of 27.80º and 46.21º which might be due to the presence of trimethyl chitosan in the sample [36].

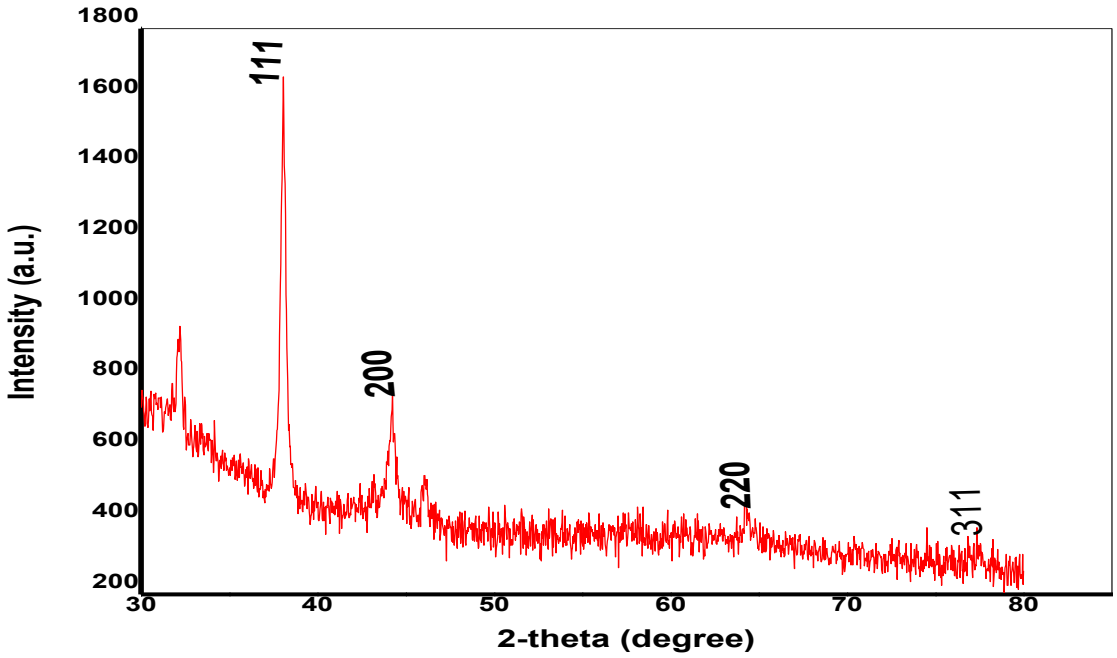

Fig. 5 X-Ray Diffraction (XRD) patterns of QTMC-AgNPs

The SEM micrograph of QTMC at image focus zoom of 10 and 5 µm (Fig. 6a and b) depicts a fine uniformly distributed cubic like images. This significant morphological change confirmed the successful methylation of CTS with high degree of methylation. In addition, morphological characteristics as demonstrated by SEM analysis revealed the high crystallinity of QTMC. Fig. 6c and d shows the SEM images of the QTMC-AgNPs at image focus zoom of 10 µm and 5 µm. The images revealed uniformly distributed spherical

shapes. This morphological behavior has been reported to be common to silver nanoparticles in previous studies [6,17,20,34].

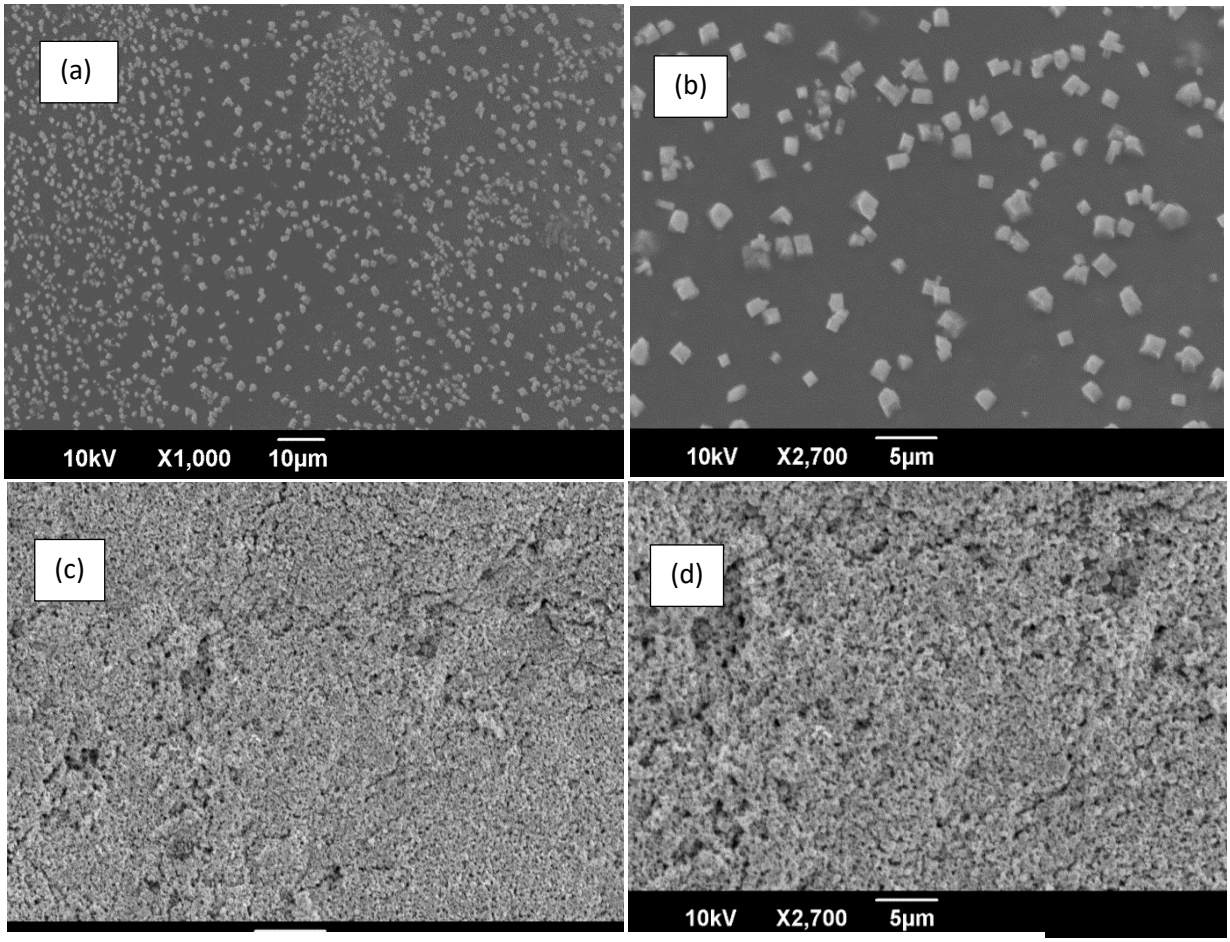

Fig. 6 SEM micrographs of (a) QTMC at image focus zoom of 10 µm (b) QTMC at image focus zoom of 5 µm (c) QTMC-AgNPs image focus zooms of 10 µm (d) QTMC-AgNPs image focus zooms of 5 µm

The EDS spectrum of QTMC-AgNPs confirmed the presence of signals characteristics of silver, carbon and oxygen. The spectrum showed the presence of Ag signal (84.47% abundance) in QTMC-AgNPs (Fig. 7), suggesting that QTMC-AgNPs were formed. The metallic Ag nanocrystals exhibited a typical optical absorption peak at exactly 3.0 keV because of surface plasmon resonance. The spectra signals obtained for oxygen (O) and carbon (C) indicate that the organic moieties from QTMC were observed on the surface or in the environment of the metallic QTMC-AgNPs. The presence of copper (Cu) signal was as a result of Cu grid used during the preparation of the sample for analysis.

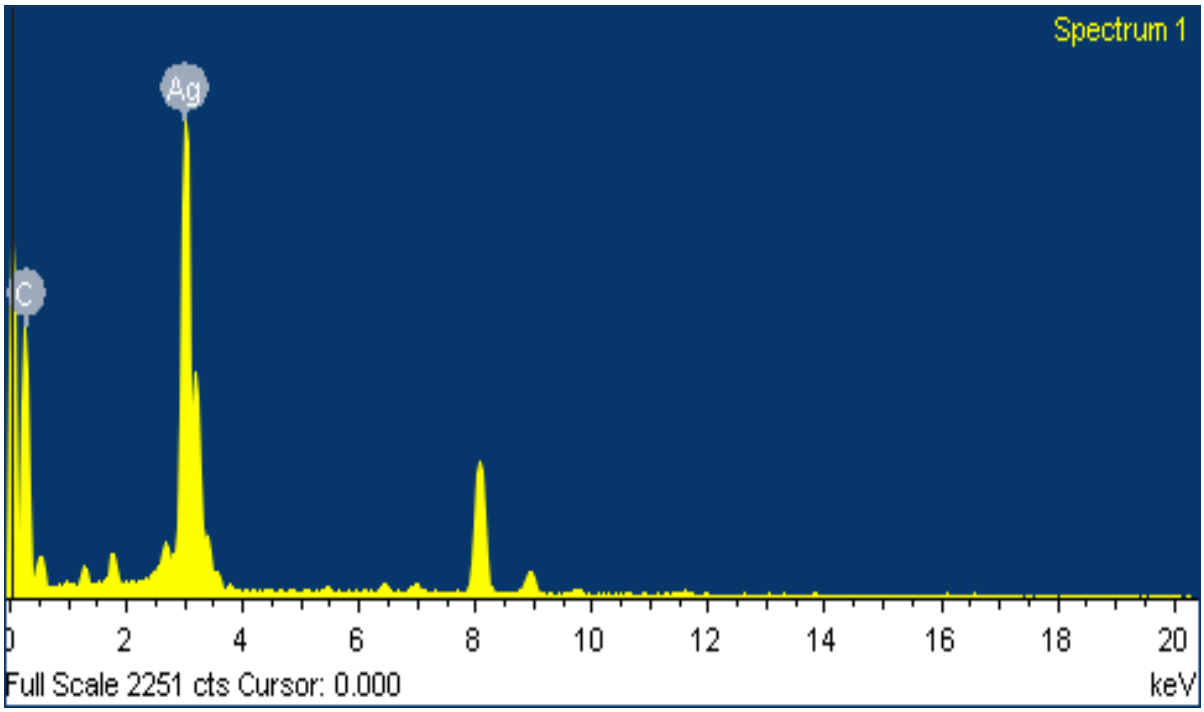

Fig. 7 EDS spectrum of QTMC-AgNPs

High-resolution TEM images of QTMC-AgNPs at image focus zoom of 20 nm and 10 nm revealed that the synthesized QTMC-AgNPs are mainly spherical and consisted of well-ordered single crystals with distinct lattice fringes (Fig. **8**a and b). The average particle size as calculated by image J software is 10 nm in diameter suggesting that the QTMC-AgNPs are very small in size. The particle size obtained in this study is very small compared to the silver nanoparticles synthesized by Chang and co-workers [**17**] in which a particle size of 60 nm in diameter was obtained. This particle size is also in good agreement with the average particles size obtained from DLS analysis (Fig. **8**e). The presence of clear and uniform lattice fringes confirmed that the spherical particles were highly crystalline. The HR-TEM images as illustrated in Fig. **8**c displayed D-spacing of 2.03 Å which corresponds to the inter-planar spacing crystalline phase of the (200) reflection plane of Ag **[31]** and the value obtained using Gatan Digital Micrograph Software is almost the same with one of the reported values for the most intense d-spacings, namely, 2.36, 2.04 and 1.44 Å of zerovalent Ag [**31**, **37**]. **Fig. 8**d shows the indexed Selected Area of Electron Diffraction (SAED) patterns, which exhibited bright circular spots that correspond to the (111), (200), and (311) reflection planes. The diffraction rings also suggest that the particles were polycrystalline. The SAED and lattice fringes of these nanocomposites are in good agreement with the XRD analysis obtained (Fig. **5**). The DLS spectrum in Fig. **8**e revealed the histogram of particle size distribution recorded from QTMC-AgNPs solutions. The

stabilized silver nanoparticles obtained were apparently nanoparticulate with average particle size of 12.5 nm [31].

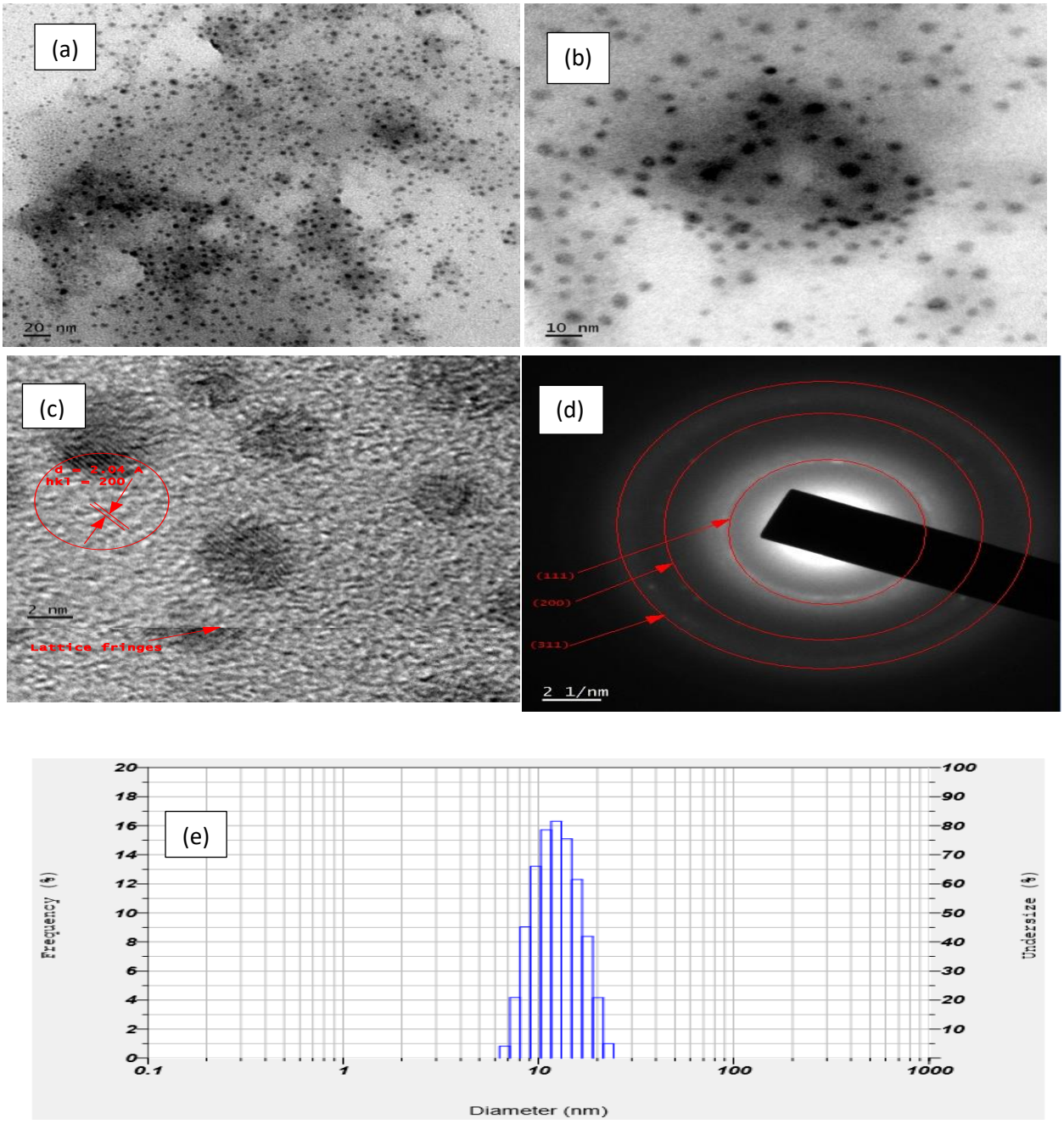

Fig. 8 (a) HR-TEM image of QTMC-AgNPs at image focus zoom of 20 nm(b)HR-TEM image of QTMC-AgNPs at image focus zoom of 10 nm zoom(c) D- spacing and lattice Fringes of QTMC-AgNPs (d) HR-TEM SAED patterns of indexed QTMC-AgNPs (e) DLS histogram of QTMC-AgNPs

The XPS analysis was performed to elucidate the elemental composition, chemical state and the environment of QTMC-AgNPs. Fig. 9a shows a typical XPS spectrum of QTMC-AgNPs nanocomposites in the range of 0-1100 eV. It reveals element such as silver (**Ag 3d**), nitrogen (**N 1s**), chlorine (**Cl 2p**), oxygen (**O 1s**) and carbon (**C 1s**). Fig. 9b shows the XPS spectrum of **Ag 3d** core level of QTMC-AgNPs with corresponding binding energies. The two high intensity peaks observed at binding energies of 366.7 eV and 373.1 eV can be ascribed to 3d region of QTMC-AgNPs which appear as a result of spin orbital splitting correspond to the core levels of **Ag 3d**$_{5/2}$ and **Ag 3d**$_{3/2}$ peaks, respectively [38, 39]. XPS spectra demonstrate a strong signal of silver nanoparticles, confirming that pure silver was present without impurities. Apparently, the result obtained in XPS analysis is consistent with XRD and literatures thereby suggest that a purified QTMC-AgNPs colloidal formation was successfully carried out.

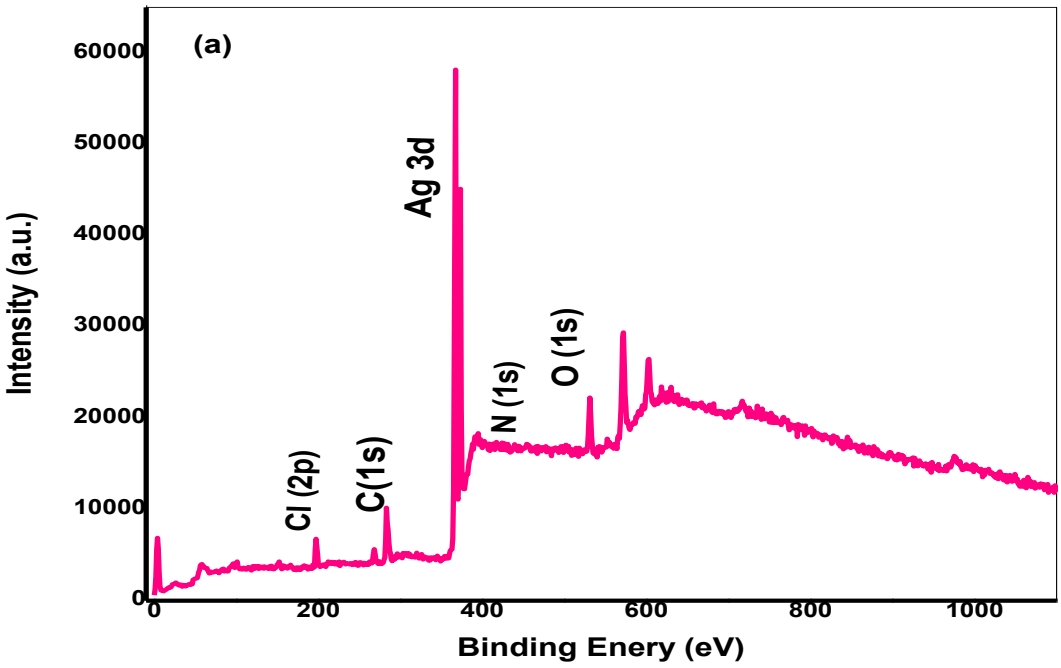

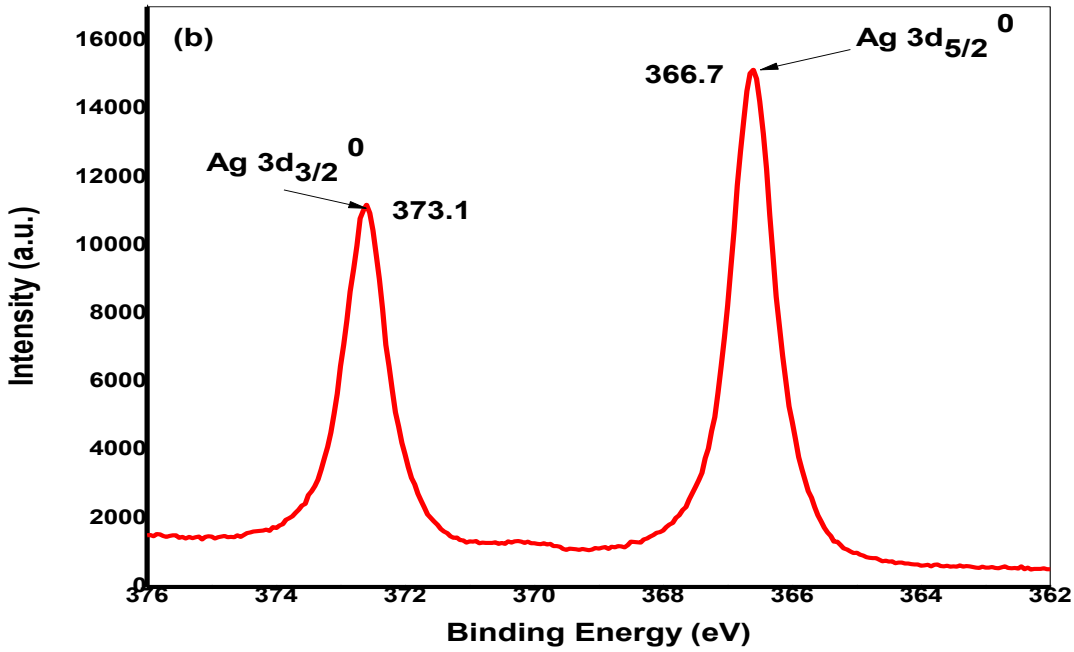

Fig. 9 XPS spectra of (a) QTMC-AgNPs (b) Ag 3d core levels of QTMC-AgNPs

The thermogravimetric (TGA/DTG) profiles of QTMC as depicted in Fig. 10a, revealed that the first thermal event occurs in the range of 50–125 ℃, which accounts for the evaporation of absorbed or bonded water from the biopolymers. The degradation of QTMC polymer samples occurs in the range of 200–225 ℃. The DTG curve confirmed that QTMC (at 223.43 ℃) is thermally stable. This finding is in accordance with the report of Pardeshi and Belgamwar [16], where a value of 221.76 ℃ was observed for trimethyl chitosan.

TGA and DTG curves of well dried QTMC-AgNPs powder is given in Fig. 10b. It is observed from TGA curve that dominant weight loss of the sample occurred in temperature region between 192.97 and 460.88 ℃. The first step of the decomposition process, which occurred between 50 and 200 ℃, can be attributed to the evaporation of volatile materials such as water adsorbed on the surface of the QTMC-AgNPs. A further degradation, with an associated weight loss of about 5.06%, was observed between 200 and 350 ℃, which is a consequence of desorption of the organic biomolecules (from QTMC) present at the surface of the nanoparticles. This weight loss might be attributed to the decomposition of trimethyl chitosan and are responsible for the stabilization of AgNPs [36]. Above 460.88 ℃, a steady weight loss accounting for about 9.893% was recorded, which could probably be assigned to the thermal degradation of resistant aromatic compounds present on the surface of the silver nanoparticles. The TGA data clearly indicated that

the QTMC are attached to the surface of the obtained nanoparticles and the organic shell was found to be 25.40 %. These results are in agreement with those reported by other studies [36].

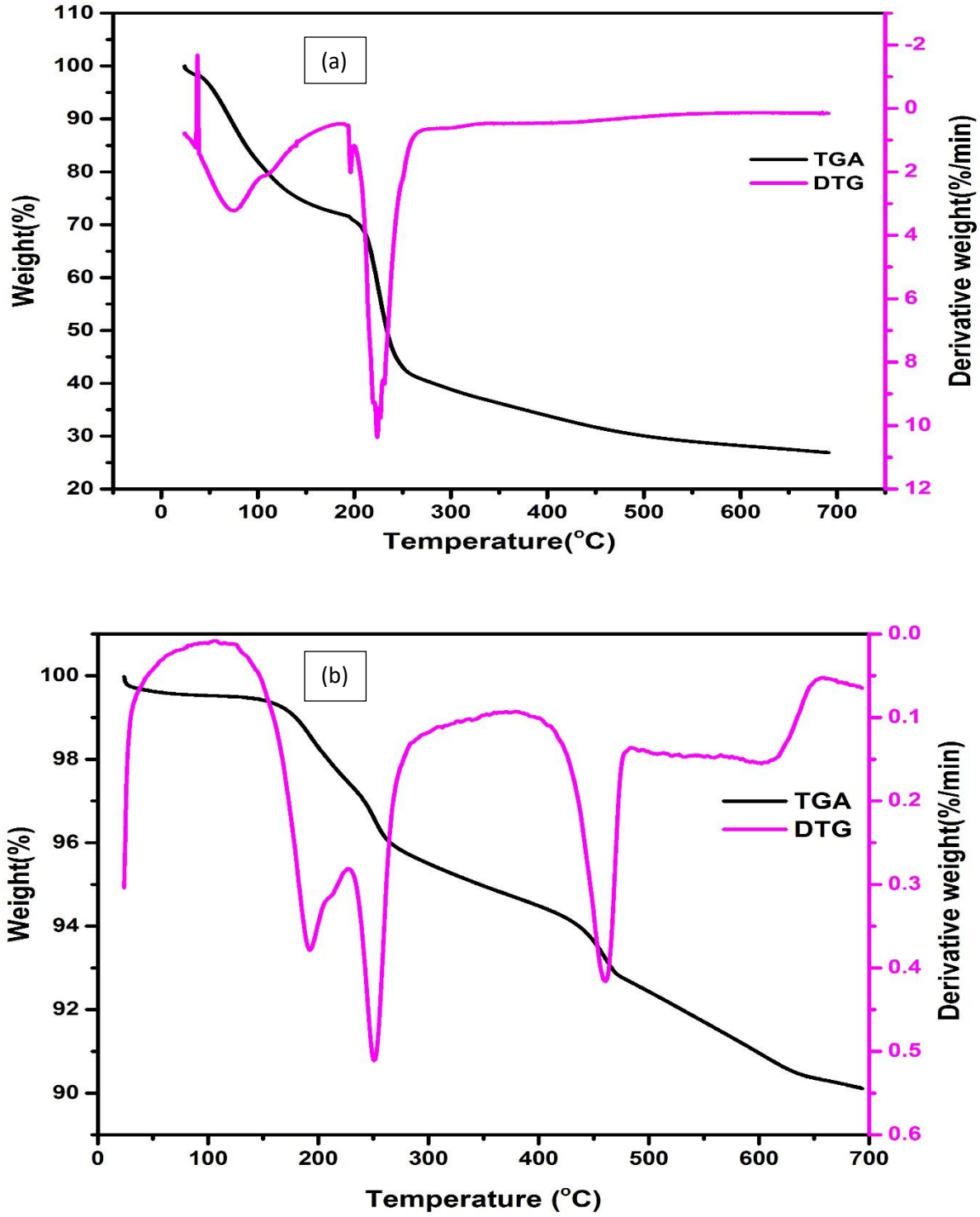

Fig. 10 TGA/DTG curves of (a) QTMC (b) QTMC-AgNPs

3.2 Antibacterial activity

The antibacterial activity of QTMC and QTMC-AgNPs were determined against gram-negative bacteria; *E. coli* and gram-positive *S. aureus*. The visible clear zone of inhibition produced by QTMC-AgNPs against *E. coli* and *S. Aureus are* shown in Fig. **11**. The presence of visible clear zones (30 mm for *E. Coli* and 26 mm for *S. Aureus*) around the QTMC-AgNPs disk suggest that the QTMC-AgNPs possessed a very high antibacterial activity which is able to inhibit the growth of both the gram-negative *E. Coli*. and gram-positive *S. Aureus*. QTMC-AgNPs showed a unique MIC value of 0.49±0.05 µg/mL for *E. Coli* whereas the MIC for *S. Aureus* was 0.98±0.02 µg/mL (Fig. **12**). It is imperative to note that the presence of QTMC in the preparation of QTMC-AgNPs has a direct effect on the activity of synthesized QTMC-AgNPs towards the two tested bacteria [**11**, **40**]. Based on the MIC and qualitative study (zone of inhibition) results, the antibacterial activities of QTMC-AgNPs are very promising. The study also compared the efficacy of synthesized QTMC-AgNPs with some reported works on antibacterial activity of silver nanoparticles (Table **1**). Shahverdi and co-workers [**41**] synthesized and investigated antibacterial activity of spherical silver nanoparticles, the team reported zone of inhibition of 9-37 mm for *E. coli* and 9-36 mm for *S. aureus*. In a related study, where polyvinylpyrrolidone was employed to cap silver nanoparticles, MIC of 1 µg/mL and 2 µg/mL were reported for *E. coli* and *S. aureus* respectively [**42**]. More so, Aazam and Zaheer [**43**] reported inhibition zone of 13 mm for *E. coli* and 10 mm for *S. aureus*. In addition, Chang and co-workers [**17**] employed TMCN to stabilize colloidal silver nanoparticles during synthesis and reported MIC of 6.13 µg/mL for both *E. coli* and *S. aureus*. Shanmugaiah and co-workers [**44**] in the same vein synthesized silver nanoparticles and evaluated the MIC to be 10 µg/mL for *E. coli* and 20 µg/mL for *S. aureus*. In a related study however, Wu and co-workers [**45**] synthesized 2.3 nm in diameter spherically shaped silver nanoparticles and reported MIC of 7.8µg/mL for both *E. coli* and *S. aureus* while zone of inhibition of 19.5 mm and 18.8 mm were reported for *E. coli* and *S. aureus* respectively. Finally, in a study where silver nanoparticles were synthesized via green approach, MIC of 3.6 µg/mL was reported for clinical isolated *E. coli* [**46**]. Comparing all the aforementioned studies with this present work, it is obvious that QTMC-AgNPs exhibited a very promising antibacterial activity. As shown in the zone of inhibition images (Fig. **11**), the antimicrobial activity was higher for the synthesized QTMC-AgNPs than all the referenced research works (Table **1**).

Another intriguing observation from the MIC results is high susceptibility of gram-negative bacteria (*E. coli*) compared with gram-positive (*S. aureus*), the growth of gram-positive bacteria is inhibited at higher concentrations of QTMC-AgNPs. Mai-prochnow and co-workers [**47**] reported similar results, emphasizing on the higher susceptibility of gram-negative bacteria in comparison with gram-positive bacteria. In the reviewed paper of Slavin and co-workers [**40**], it is hypothesized that the higher susceptibility of gram-

negative bacteria could be attributed to differences in the arrangement of bacterial cell wall, cell physiology, metabolism or degree of contact. In the case of gram-negative bacteria such as *E. coli*, the peptidoglycan component is made up of 8 nm by diameter thin layer with an additional layer of lipopolysaccharides (1–3 µm thick). This phenomenon may account for the high toxicity of QTMC-AgNPs observed against gram-negative *E. coli* over gram-positive *S. aureus*. On the other hand, gram-positive bacteria such as *S. Aureus* possess a peptidoglycan layer which is much thicker than gram-negative bacteria, spanning over 80 nm in diameter. The antibacterial activity of this prepared QTMC-AgNPs may be due to proposed bimodal mechanism of action which is in variance with that associated with conventional antibiotics.

Table 1

Comparing the *In Vitro* antibacterial activity (MIC, µg/mL or ZOI, mm) of QTMC-AgNPs against *E. coli* and *S. aureus* with antibacterial activities of selected reported works on silver nanoparticles

AgNPs (nm)	Shape	Pathogen	Exposure Time (h)	Antibacterial Activity (µg/mL/mm)	Capping Agent	Reference
10	**Spherical**	***E. coli***	**24**	**MIC = 0.49, ZOI = 30**	**QTMC**	**PS**
		S. aureus		**MIC = 0.98, ZOI = 26**		
60	Spherical	*E. coli*	24	MIC = 6.13	TMCN	[17]
		S. aureus		MIC = 6.13		
5-10	Spherical	*E. coli*	24	ZOI = 13		[43]
		S. aureus		ZOI = 10		
7.1	Spherical	*E. coli*	18	MIC = 3.6		[46]
22.5	Spherical	*E. coli* (CI)	24	ZOI = 9 – 37		[41]
		S. aureus (CI)		ZOI = 9 – 36		
2.3	Spherical	*E. coli*	24	MIC = 7.8, ZOI = 19.5	Citrate	[45]
		S. aureus		MIC = 7.8, ZOI = 18.8		
5	Spherical	*E. coli*	24	MIC = 1	PVP	[42]
		S. aureus		MIC = 2		

PS = Present Study, CI = Clinical Isolate, TMCN = trimethyl chitosan nitrate, PVP = polyvinylpyrrolidone, MIC = Minimum Inhibitory concentration, ZOI = Zone of Inhibition.

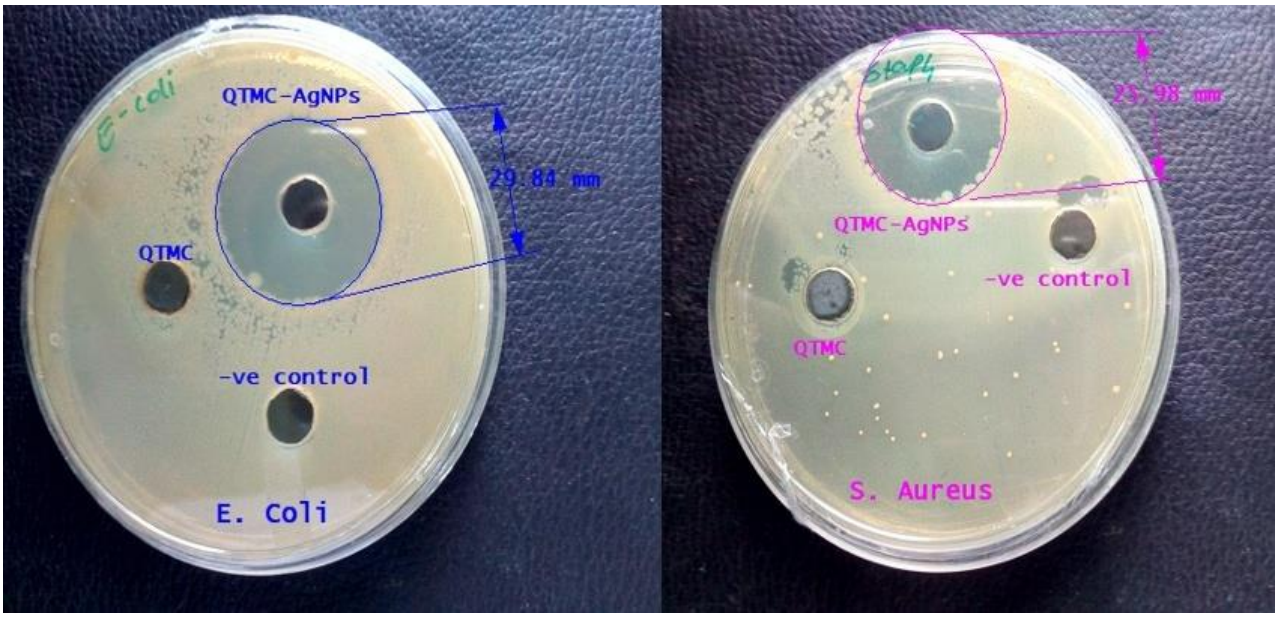

Fig.11 Disk diffusion susceptibility of QTMC and QTMC-AgNPs against *E. coli* and *S. aureus*

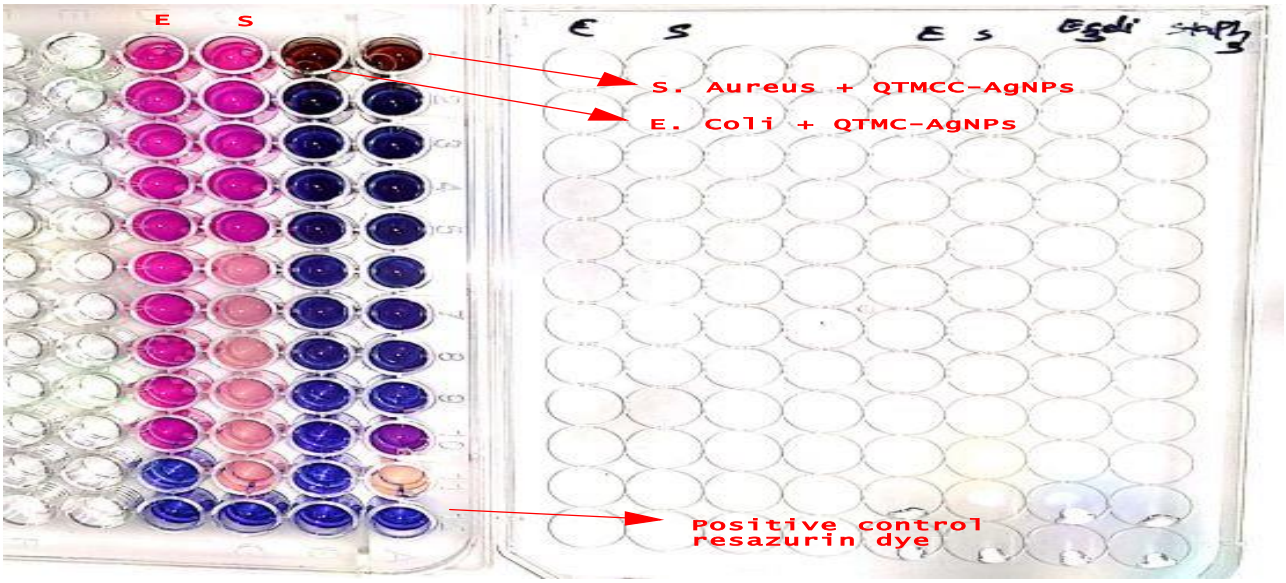

Fig. 12 MIC and MBC result of QTMC-AgNPs against *E. coli* and *S. aureus*

3.3 Antifungal activity

The antifungal activity of QTMC and QTMC-AgNPs are evaluated against two plant pathogens (S. *rolfsii and* F. *oxysporum*). The QTMC-AgNPs displayed good antifungal properties, as the concentration of 50 µg/mL had 100% growth inhibition of *S.rolfsii*, whereas growth inhibition of 76.67% was recorded against *F.oxysporum* (Fig. 13c and d). In contrast, the disk without QTMC-AgNPs shows zero efficacy against the two selected plant pathogens (Fig. 13a and b). The percentage growth of inhibition was obtained according

to Eq. 1. Several synthesized AgNPs have shown antifungal activities against different plant pathogen [5, 48, 49]. Briefly, Karma and Dutta [50] reported antifungal activity of biologically synthesized silver nanoparticles and growth inhibition was found to be 78.36% and 72.44% against *S. rolfsii* and *F. oxysporum* respectively at concentration of 100 µg/mL. In a related literature, Al abboud [51] investigated the antifungal activity of biologically synthesized silver nanoparticles and 100 % growth inhibition was observed against *F. oxysporum* at concentration of 80 µg/mL. It has been reported that nanoparticles have the capability to disrupt both fungal cell walls and membranes thereby leading to leakage of intracellular components that may cause sudden death of the fungi [30]. They can also ensure fungal death through the generation of reactive oxygen species and hydroxyl radicals. QTMC on the other hand did not give any noticeable antifungal properties against the two selected plant pathogens. This unique phenomenon of the prepared QTMC-AgNPs can be attributed to its smaller size and good particle sizes distribution.

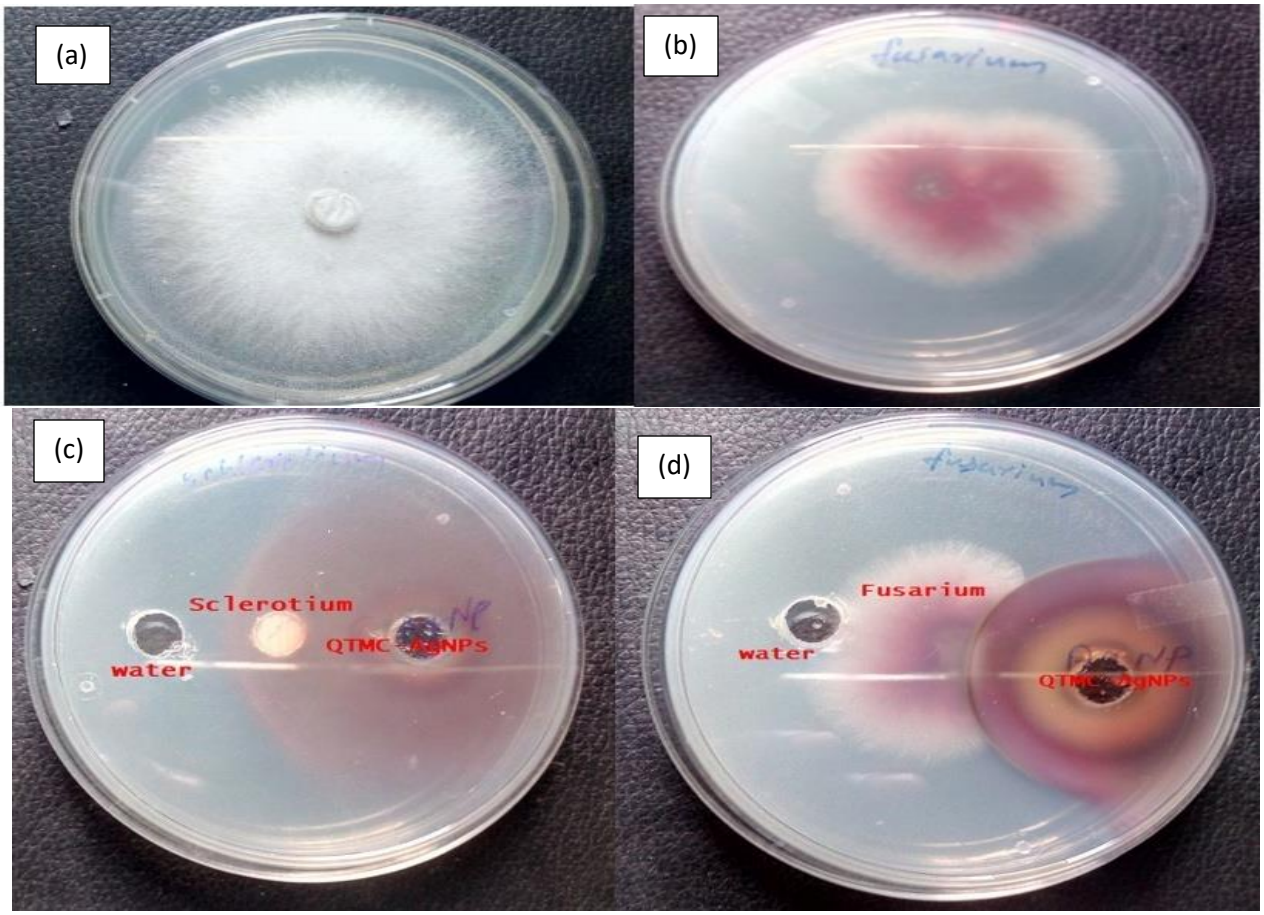

Fig. 13 (a) Negative control of *S.rolfsii* (b) Negative control of *F.oxysporum* (c) Antifungal activity of QTMC-AgNPs against *S.rolfsii* (d) Antifungal activity of QTMC-AgNPs against *F.oxysporum.*

4 Conclusion

This study demonstrated two steps reductive methylation of CTS in a controlled system and represents a chemically modified derivative of CTS with enhanced solubility at wide pH. The study further demonstrated that QTMC-AgNPs, can be prepared in an environmentally friendly manner by the chemical reduction of silver ions in an agitated aqueous medium below room temperature without heating or photo-radiation. Accordingly, it was found that the synthesized QTMC-AgNPs with positively charged surfaces inhibited/killed the growth of gram-negative bacteria; *E. coli* and and gram-positive; *S. aureus* at a very low concentration with improved activity when compared with some related reported studies. Also, the high susceptibility of gram-negative, *E. coli* over gram-positive, *S. aureus* was established. The study also revealed that QTMC-AgNPs was highly effective against two selected plant pathogen, *S .rolfsii* and *F. oxysporum* while ordinary QTMC had zero efficacy. The broad-spectrum antibacterial activity of QTMC-AgNPs against the selected gram-positive and gram-negative bacteria could be translated into clinical therapy, especially considering the shortage of new antibiotics for controlling multi drug resistance bacterial. Complementally, can be a good alternative candidate as antifungal agent against the multidrug-resistant strains of plant fungi.

Declaration of Competing Interest

The authors declare no conflict of interest

Acknowledgements

Yakubu Adekunle Alli acknowledges Peculiar Consult and Peculiar Ultimate Concerns Limited for sponsoring his research trip to International and Inter University Centre for Nanoscience and Nanotechnology (IIUCNN), Mahatma Gandhi University, Kottayam, Kerala, India. He also appreciates the center (IIUCNN) for providing advanced characterization techniques as well as Microbiology Department, School of Bioscience Mahatma Gandhi University, Kottayam, Kerala, India for assisting in antimicrobial tests.

References

[1] S.I. Hay, P. C. Rao, C. Dolecek, N. P. J. Day, A. Stergachis, A. D. Lopez, C. J. L. Murray, Measuring and mapping the global burden of antimicrobial resistance. BMC Med. **16,** 78(2018)

[2] World Health Organization, Antimicrobial Resistance: Global Report on Surveillance, 2014.

[3] L. J. Shallcross, S. J. Howard, T. Fowler, S. C. Davies, Tackling the threat of antimicrobial resistance: from policy to sustainable action. Philosophical Transactions of the Royal Society B: Biological Sciences **370**, 20140082–20140082 (2015)

[4] J. 0'Neil, House of Common Library. CDP2017/0074(2017)

[5] G. D. Kumar, N. Natarajan, S. Nakkeeran, Synthesis and characterization of silver (Ag) nanoparticles and Its antifungal activity Against Sclerotiumrolfsii in chilli (Capsicum annum L.). Int. J. Agric. Sci. Res. **5**(3), 211-218(2016).

[6] Y. Y. Loo, Y. Rukayadi, M-A-R. Nor-Khaizura, C. H. Kuan, B. W. Chieng, M. Nishibuchi, S. Radu, In Vitro Antimicrobial Activity of green synthesized silver nanoparticles against selected gram-negative foodborne pathogens. Front. Microbiol. **9**, 1555 (2018)

[7] S. H. Lee, B. A. Jun, Silver nanoparticles: synthesis and application for nanomedicine. Int. J. Mol. Sci. **20**(4), 865 (2019)

[8] T. Chivangkul, S. Pengprecha, P. Padungros, K. Siraleartmukul, S. Prasongsuk, N. Muangsin, Enhanced water-solubility and mucoadhesion of N,N,N-trimethyl-N-gluconate-N-homocysteine thiolactone chitosan. Carbohydr. Polym. **108**, 224–231 (2014)

[9] A. Ahmad, N. Mubharak, K. Naseem, H. Tabassum, M. Rizwan, A. Najda, M. Khasif, M. Bin-Jumah, A. Hussain, A. Shaheen, M. M. Abdel-Daim, S. Alli, S. Hussain, Recent Advancement and development of chitin and chitosan -based nanocomposite for Drug Delivery: Critical approach to clinical research. Arabian J. Chem. (2020). doi:10.1016/j.arabjc.2020.10.019

[10] M. Ottonelli, S. Zappia, A. Demartini, M. Alloisio, Chitosan-stabilized noble metal nanoparticles: study of their shape evolution and post-functionalization properties. Nanomaterials (Basel) **10**(2), 224 (2020)

[11] J. Li, S. Zhuang, Antibacterial activity of chitosan and its derivatives and their interaction mechanism with bacteria: Current state and perspectives. Eur. Polym. J. **138**, 109984 (2020)

[12] S. Adewuyi, K. T. Kareem, A. O. Atayese, S. A. Amolegbe, C. A. Akinremi, Chitosan-bound pyridinedicarboxylate Ni(II) and Fe(III) complex biopolymer films as waste water decyanidation agents. Int. J. Biol. Macromol. **48**, 301-303 (2011)

[13] I. Younes, M. Rinaudo, Chitin and chitosan preparation from marine sources. structure, properties and applications. Mar. Drugs **13**(3), 1133–1174 (2015)

[14] S. Adewuyi, J. M. Jacob, O. O. Olaleye, T. O. Abdulraheem, J. A. Tayo, F. O. Oladoyinbo, Chitosan-bound pyridinedicarboxylate Ni(II) and Fe(III) complex biopolymer films as waste water decyanidation agents. Carbohydr. Polym. **151**, 1235─1239 (2016)

[15] H. F. G. Barbosa, M. Attjioui, A. P. G. Ferreira, E. R. Dockal, N. E. El Gueddari, B. M. Moerschbacher, É. T. G. Cavalheiro, Synthesis, characterization and biological activities of biopolymeric schiff bases prepared with chitosan and salicylaldehydes and their Pd(II) and Pt(II) complexes. Molecules **22**(11), 1987 (2017)

[16] C. V. Pardeshi, V. S. Belgamwar, Controlled synthesis of N,N,N-trimethyl chitosan for modulated bioadhesion and nasal membrane permeability. Int. J. Bio. Macromol. **82**, 933–944 (2016)

[17] T. C. Chang, C. C. Chen., K. M. Cheng, C. Y. Chin, Y. H. Chen, X. A. Chen, J. R. Sun, J. J. Young, T. S. Chiueh, Trimethyl chitosan-capped silver nanoparticles with positive surface charge: their catalytic activity and antibacterial spectrum including multidrug-resistant strains of Acinetobacterbaumannii. Colloids Surf., B **155**, 61-70 (2017)

[18] A. D. Kulkarni, H. M. Patel, S. J. Surana, S. J. Y. H. Vanjari, V. S. Belgamwar, C. V. Pardeshi, N,N,N -Trimethyl chitosan: An advanced polymer with myriad of opportunities in nanomedicine. Carbohydr. Polym. **157**, 875–902 (2017)

[19] A. B. Sieval, M. Thanoual, A. F. Kotze, J. C. Verhoef, J. Brussee, H. E. Junginger, Preparation and NMR characterization of highly substituted N-trimethyl chitosan chloride. Carbohydr. Polym. **36**, 157-165 (1998)

[20] Y. Ding, X. Xia, X. C. Zhang, Synthesis of metallic nanoparticles protected with N,N,N-trimethyl chitosan chloride via a relatively weak affinity. Nanotechnolog. **17**, 4156-4162 (2006)

[21] Y. A. Alli, R. Bello, S. Adewuyi, T. Sabu, H. Anuar, Bismuth nanoparticles capped cationic quaternary trimethyl chitosan: Synthesis, antibacterial and catalytic activities. TB-ART-06-2021-001246, *J. Mater. Chem. B*, (Submitted)

[22] B. F. C. A. Gohin, H. Zeng, S. Xu, K. Zou, B. Liu, X. Li. Huang, X. Cao, Optimization of ZnAl/chitosan supra-nano hybrid preparation as efficient antibacterial material. Int. J. Mol. Sci. **20**, 5705 (2019)

[23] T. Roshmi, K. R. Soumya, M. Jyothis, E. K. Radhakrishnan, Effect of biofabricated gold nanoparticle-based antibiotic conjugates on minimum inhibitory concentration of bacterial isolates of clinical origin. Gold Bull. **48**(1-2), 63-71 (2015)

[24] R. Thomas, K. R. Soumya, J. Mathew, J. E.K Radhakrishnan, Inhibitory effect of silver nanoparticle fabricated urinary catheter on colonization efficiency of coagulase negative staphylococci. J. Photochem. Photobiol., B **149**, 68-77 (2015)

[25] Q. Bao, D. Zhang, P. Qi, Synthesis and characterization of silver nanoparticle and graphene oxide nanosheet composites as a bactericidal agent for water disinfection. J. Colloid Interface Sci. **360**(2), 463-470 (2011)

[26] A. F. de Faria, D. S. T. Martinez, S. M. M. Meira, A. C. M. de Moraes, A. Brandelli, A. G. Souza Filho, O. L. Alves, Anti-adhesion and antibacterial activity of silver nanoparticles supported on graphene oxide sheets. Colloids Surf., B 113, 115-124 (2014)

[27] K. Ishida, T. F. Cipriano, G. M. Rocha, G. Weissmüller, F. Gomes, K. Miranda, S. Rozental, Silver nanoparticle production by the fungus Fusariumoxysporum: nanoparticle characterisation and analysis of antifungal activity against pathogenic yeasts. Mem. Inst. Oswaldo Cruz **109**(2), 220-228 (2014)

[28] N. V. Ayala-Núñez, H. H. L. Villegas, L. D. C. I. Turrent, C. R. Padilla, Silver nanoparticles toxicity and bactericidal effect against methicillin-resistant Staphylococcus aureus: nanoscale does matter. Nanobiotechnology **5**(1-4), 2-9 (2009)

[29] M. Khatami, S. Pourseyedi, M. Khatami, H. Hamidi, M. Zaeifi, L. Soltani, Synthesis of silver nanoparticles using seed exudates of *Sinapisarvensis* as a novel bioresource, and evaluation of their antifungal activity. Bioresour. Bioprocess. **2**, 19 (2015)

[30] A. Lateef, B. I. Folarin, S. M. Oladejo, P. O. Akinola, L. S. Beukes, E. B. Gueguim-Kana, Characterization, antimicrobial, antioxidant, and anticoagulant activities of silver nanoparticles synthesized from Petiveriaalliacea L. leaf extract. Prep. Biochem. Biotechnol. **48**(7), 646-652 (2018).

[31] H. Peng, Y. Liu, W. Peng, J. Zhang, R. Ruan, Green synthesis and evaluation of Ag nanoparticles using bamboo hemicellulose. BioResources **11**(1), 385-399 (2016)

[32] A.F. Martins, J. F. Piai, I. T. A. Schuquel, A. F. Rubira, E. C. Muniz, Polyelectrolytes complexes of chitosan/heparin and N,N,N-trimethylchitosan/heparin obtained at different pH: Preparation, characterization and controlled release of heparin. Colloid Polym. Sci. **289**, 1133–1144 (2011)

[33] JCPDS, Joint Committee for Powder Diffraction Standards. Power diffraction file for inorganic materials, 1979

[34] S. Mickmaray, One-step synthesis of silver nanoparticles using Saudi Arabian desert seasonal plant sisymbriumirio and antibacterial activity against multidrug-resistant bacterial strains. Biomolecules **9**(11), 662 (2019)

[35] J. L. López-Miranda, M. Vázquez, N. Fletes, R. Esparza, G. Rosas, Biosynthesis of silver nanoparticles using a *Tamarixgallica* leaf extract and their antibacterial activity. Mater. Lett. **176**, 285–289 (2016)

[36] L. David, B. Moldovan, Green synthesis of biogenic silver nanoparticles for efficient catalytic removal of harmful organic dyes. Nanomaterials **10**, 202 (2020)

[37] E. E. Abdel-Halim, S. S. Al-Deyab, Utilization of hydroxypropyl cellulose for green and efficient synthesis of silver nanoparticles. Carbohydr. Polym. **86**(4), 1615-1622 (2011)

[38] S. Liang, G. Zhang, J. Min, J. Ding, X. Jiang, Synthesis and antibacterial testing of silver/poly (ether amide) composite nanofibers with ultralow silver content. J. Nanomater. **2014**,1–10 (2014)

[39] Á. de J. Ruíz-Baltazar, S. Y. Reyes-López, M. de L. Mondragón-Sánchez, M. Estevez, A. R. Hernández-Martinez, R. Pérez, Biosynthesis of Ag nanoparticles using Cynaracardunculus leaf extract: Evaluation of their antibacterial and electrochemical activity. Results Phys. **11**, 1142–1149 (2018)

[40] Y. N. Slavin, J. Asnis, U. O. Häfeli, H. Bach, Metal nanoparticles: understanding the mechanisms behind antibacterial activity. J. Nanobiotechnol. **15**, 65 (2017)

[41] A. R. Shahverdi, A. Fakhimi, H. R. Shahverdi, S. Minaian, Synthesis and effect of silver nanoparticles on the antibacterial activity of different antibiotics against *Staphylococcus aureus* and *Escherichia coli*. Nanomedicine: Nanotechnology, Biology and Medicine **3**(2), 168–171 (2007)

[42] W. Li, T. Sun, S. Zhou, Y. Ma, Q. Shi, X. Xie, X. Huang, A comparative analysis of antibacterial activity, dynamics, and effects of silver ions and silver nanoparticles against four bacterial strains. Int. Biodeterior. Biodegrad. **123**, 304-310 (2017)

[43] E.S Aazam Z. Zaheer, Growth of Ag-nanoparticles in an aqueous solution and their antimicrobial activities against Gram positive, Gram negative bacterial strains and Candida fungus. Bioprocess Biosyst Eng. **39**(4), 575–584 (2016)

[44] V. Shanmugaiah, H. Harikrishnan, N. Sal-harbi, K. Shine, J. M. Khaled, N. Balasubramanian, R. shyamkumar, Facile synthesis of silver nanoparticles using streptomycessp. vsmgt1014 and their antimicrobial efficiency. Digest J. Nanomat. Biostructures **10**, 179-187 (2015)

[45] Y. Wu, Y. Yang, Z. Zhang, Z. Wang, Y. Zhao, L. Sun, A facile method to prepare size-tunable silver nanoparticles and its antibacterial mechanism. Adv. Powder Technol, **29**(2), 407–415 (2018)

[46] B. Ramalingam, T. Parandhaman, S. K. Das, Antibacterial effects of biosynthesized silver nanoparticles on surface ultrastructure and nanomechanical properties of gram-negative bacteria viz. Escherichia coli and Pseudomonas aeruginosa. ACS Appl. Mater. Interfaces **8**(7), 4963–4976 (2016).

[47] A. Mai-Prochnow, M. Clauson, J. Hong, A. B. Murphy, Gram-positive and Gram-negative bacteria differ in their sensitivity to cold plasma. Sci. Rep. **6**, 38610 (2016)

[48] J. G. Fernandez, M. A. Fernandez-Baldo, E. Berni, G. Camı, N. Duran, J. Raba, M. I. Sanz, Production of silver nanoparticles using yeasts and evaluation of their antifungal activity against phytopathogenic fungi. Biochem. **51**, 1306–1313 (2016)

[49] K-J. Kim, W. S. Sung, B. K. Suh, S. K. Moon, J. S. Choi, J. G. Kim, D. G. Lee, Antifungal activity and mode of action of silver nano-particles on Candida albicans. Biometals. **22**, 235–242 (2009)

[50] P. K. Kaman, P. Dutta, Synthesis, characterization and antifungal activity of biosynthesized silver nanoparticle. Indian Phytopathol. **72**, 79-88 (2019)

[51] M. A. Al Abboud, Fungal biosynthesis of silver nanoparticles and their role in control of fusarium wilt of sweet pepper and soil-borne fungi in vitro. Int. J. Pharmacol. **14**, 773–780 (2018)